Eur. Phys. J. A (2013) **49**: 49
DOI 10.1140/epja/i2013-13049-0

THE EUROPEAN PHYSICAL JOURNAL A

Regular Article – Experimental Physics

The neutron-proton charge-exchange amplitudes measured in the dp → ppn reaction

D. Mchedlishvili[1,2], S. Barsov[3], J. Carbonell[4], D. Chiladze[1,2], S. Dymov[5,6], A. Dzyuba[3], R. Engels[2], R. Gebel[2], V. Glagolev[7], K. Grigoryev[2,3], P. Goslawski[8], M. Hartmann[2], A. Kacharava[2], V. Kamerdzhiev[2], I. Keshelashvili[1,9], A. Khoukaz[8], V. Komarov[5], P. Kulessa[10], A. Kulikov[5], A. Lehrach[2], N. Lomidze[1], B. Lorentz[2], G. Macharashvili[1,5], R. Maier[2], S. Merzliakov[2,5], M. Mielke[8], M. Mikirtychyants[2,3], S. Mikirtychyants[2,3], M. Nioradze[1], H. Ohm[2], M. Papenbrock[8], D. Prasuhn[2], F. Rathmann[2], V. Serdyuk[2], H. Seyfarth[2], H.J. Stein[2], E. Steffens[6], H. Stockhorst[2], H. Ströher[2], M. Tabidze[1], S. Trusov[11], Yu. Uzikov[5,12], Yu. Valdau[2,3], and C. Wilkin[13,a]

[1] High Energy Physics Institute, Tbilisi State University, GE-0186 Tbilisi, Georgia
[2] Institut für Kernphysik and Jülich Centre for Hadron Physics, Forschungszentrum Jülich, D-52425 Jülich, Germany
[3] High Energy Physics Department, Petersburg Nuclear Physics Institute, RU-188350 Gatchina, Russia
[4] Institut de Physique Nucléaire, Université Paris-Sud, IN2P3-CNRS, F-91406 Orsay Cedex, France
[5] Laboratory of Nuclear Problems, JINR, RU-141980 Dubna, Russia
[6] Physikalisches Institut II, Universität Erlangen–Nürnberg, D-91058 Erlangen, Germany
[7] Laboratory of High Energies, JINR, RU-141980 Dubna, Russia
[8] Institut für Kernphysik, Universität Münster, D-48149 Münster, Germany
[9] Department of Physics, University of Basel, Klingelbergstrasse 82, CH-4056 Basel, Switzerland
[10] H. Niewodniczański Institute of Nuclear Physics PAN, PL-31342 Kraków, Poland
[11] Institut für Kern- und Hadronenphysik, Forschungszentrum Rossendorf, D-01314 Dresden, Germany
[12] Department of Physics, M. V. Lomonosov Moscow State University, RU-119991 Moscow, Russia
[13] Physics and Astronomy Department, UCL, Gower Street, London, WC1E 6BT, UK

Received: 11 December 2012 / Revised: 13 March 2013
Published online: 22 April 2013

Communicated by T. Hennino

Abstract. The unpolarised differential cross section and the two deuteron tensor analysing powers A_{xx} and A_{yy} of the $\vec{d}p \to \{pp\}_s n$ charge-exchange reaction have been measured with the ANKE spectrometer at the COSY storage ring. Using deuteron beams with energies 1.2, 1.6, 1.8, and 2.27 GeV, data were obtained for small momentum transfers to a $\{pp\}_s$ system with low excitation energy. The results at the three lower energies are consistent with impulse approximation predictions based upon the current knowledge of the neutron-proton amplitudes. However, at 2.27 GeV, where these amplitudes are far more uncertain, agreement requires a reduction in the overall double-spin-flip contribution, with an especially significant effect in the longitudinal direction. These conclusions are supported by measurements of the deuteron-proton spin-correlation parameters $C_{x,x}$ and $C_{y,y}$ that were carried out in the $\vec{d}\vec{p} \to \{pp\}_s n$ reaction at 1.2 and 2.27 GeV. The values obtained for the proton analysing power A_y^p also suggest the need for a radical re-evaluation of the neutron-proton elastic scattering amplitudes at the higher energy. It is therefore clear that such measurements can provide a valuable addition to the neutron-proton database in the charge-exchange region.

1 Introduction

An understanding of the nucleon-nucleon (NN) interaction is fundamental for the whole of nuclear and hadronic physics. The SAID database and analysis program [1] have proved to be truly invaluable tools over many years for researchers working in this area. The general procedure adopted here is to take all the NN elastic scattering data in the literature in order to perform a phase shift analysis up to a certain orbital angular momentum $L_{\max}$ and use a theoretical model for higher L. When significant new experimental data become available, the value of $L_{\max}$ can be increased. By assuming that the phase shifts vary smoothly with beam energy, predictions can be made for observables at a particular energy and it is in this way that the SAID program is most commonly used.

[a] e-mail: c.wilkin@ucl.ac.uk

Clearly any amplitude analysis can only be as good as the data used in its implementation. Though lots of proton-proton observables have been measured up to high energies, there are significant gaps in our knowledge for beam energies above $\approx 2\,\mathrm{GeV}$, especially at small angles. The situation is even more serious for neutron-proton scattering where there are major holes in the experimental database above about 1 GeV and data that do exist are not necessarily very well reproduced by the SAID program. For example, the only differential cross section data for large angle np scattering [2], in the so-called charge-exchange region, seem to be consistently overpredicted in the SAID analysis.

Extra information in the np sector can be found by performing experiments with a deuteron beam or a deuterium target. The simplest of these involves measuring the ratio of the forward charge-exchange cross section of a neutron on a deuterium target to that on hydrogen,

$$R_{np}(0) = \left.\frac{\mathrm{d}\sigma(nd \to pnn)/\mathrm{d}t}{\mathrm{d}\sigma(np \to pn)/\mathrm{d}t}\right|_{\theta=0}, \qquad (1)$$

where t is the square of the four-momentum transfer between the initial neutron and final proton. Due to the Pauli principle, when the two final neutrons are in a relative S-wave their spins must be antiparallel and the system is in the $^1S_0$ state. Under such circumstances the $nd \to p\{nn\}$ reaction involves a spin flip from the $S = 1$ of the deuteron to the $S = 0$ of the dineutron. In impulse approximation the ratio determines

$$R_{np}(0) = \frac{2}{3}\left(\frac{\sigma_{sf}}{\sigma_{sf} + \sigma_{nsf}}\right), \qquad (2)$$

where σ_{sf} (σ_{nsf}) is the forward np charge-exchange differential cross section with (without) a spin-flip [3,4].

Extensive measurements of $R_{np}(0)$ have been reported and these have been extended up to 2 GeV at Dubna [5]. Although impulse approximation predictions for $R_{np}(0)$ on the basis of the current SAID amplitudes reproduce well these observations from 300 MeV up to about 800 MeV, there are serious discrepancies above 1 GeV [6]. In terms of eq. (2), it seems that the SAID solution overestimates the contribution of the spin-flip amplitudes to the forward np charge-exchange cross section.

More detailed information on the np charge-exchange amplitudes can be derived by using a polarised deuteron beam or target and studying the $\vec{d}p \to \{pp\}_s n$ reaction [7]. To achieve maximum sensitivity, the excitation energy E_{pp} in the final pp system must be very low. As already pointed out by Pomeranchuk in 1951 [8], the Pauli principle then requires the final diproton to be in the $^1S_0$ configuration with antiparallel spins. Experiments from a few hundred MeV up to 2 GeV [9,10] have generally borne out well predictions based upon the impulse approximation [7].

In order to constrain the np amplitudes using this approach, the ANKE Collaboration has embarked on a systematic programme to measure the $\vec{d}p \to \{pp\}_s n$ observables up to the maximum COSY deuteron energy of $T_d \approx 2.3\,\mathrm{GeV}$ [11]. The proof of principle of the method was the experiment carried out at a deuteron energy of 1.17 GeV where, because of the wealth of neutron-proton data, the SAID amplitudes used as input in the calculations should be quite reliable. The measured values of the unpolarised cross section and the two deuteron Cartesian tensor analysing powers A_{xx} and A_{yy} were then quantitatively reproduced in impulse approximation [12]. Dilutions of the signals due to higher partial waves in the final pp system were taken into account in the calculations [13]. The results of similar measurements are presented here at deuteron beam energies of 1.2, 1.6, 1.8, and 2.27 GeV.

We have described the phenomenology of the deuteron charge-exchange reaction at some length in earlier publications [12,14,15] but, in order to make the current paper more self-contained, some of this material is repeated in sect. 2. The experimental set-up for measuring with the hydrogen cluster-jet target is identical to that used in our earlier work [12] and so most of the emphasis in sect. 3 is on the polarised hydrogen gas cell used in the spin-correlation measurements. The measurements of the luminosity through the observation of the quasi-free $pn \to d\pi^0$ reaction are reported in sect. 4, where the results for the unpolarised $dp \to \{pp\}_s n$ differential cross sections are compared with impulse approximation calculations.

The polarisation of the deuteron beam was established at 1.2 GeV and, since there are no depolarising resonances for the deuteron in the COSY energy range, the analysing powers for the $\vec{d}p \to \{pp\}_s n$ reaction could be measured at various energies and the results are presented in sect. 5. The polarisation measurements with the gas cell have no parallel in our earlier work. The method used here relies on the data taken with the polarised deuterium target and the measurement of the analysing power of quasi-free $n\vec{p} \to d\pi^0$. Taken together with the measurement of the vector polarisation of the deuteron beam, this allowed us to extract the spin-correlation and proton analysing power results given in sect. 6. Our conclusions regarding the usefulness of charge exchange on the deuteron in the study of neutron-proton elastic scattering amplitudes are drawn in sect. 7.

2 Deuteron charge exchange in impulse approximation

The cross section and spin observables for the $dp \to \{pp\}_s n$ reaction have been extensively discussed in the literature [7,13] and only essential formulae are collected here. In impulse approximation the deuteron charge exchange amplitude is proportional to a neutron-proton charge exchange amplitude times a form factor that reflects the overlap between the initial deuteron wave function and that of the outgoing diproton system.

The elementary $np \to pn$ amplitude may be written in terms of five scalar amplitudes in the cm system as

$$f_{np} = \alpha(q) + i\gamma(q)(\boldsymbol{\sigma}_1 + \boldsymbol{\sigma}_2)\cdot\boldsymbol{n} + \beta(q)(\boldsymbol{\sigma}_1\cdot\mathbf{n})(\boldsymbol{\sigma}_2\cdot\boldsymbol{n}) + \delta(q)(\boldsymbol{\sigma}_1\cdot\boldsymbol{m})(\boldsymbol{\sigma}_2\cdot\boldsymbol{m}) + \varepsilon(q)(\boldsymbol{\sigma}_1\cdot\boldsymbol{l})(\boldsymbol{\sigma}_2\cdot\boldsymbol{l}), \qquad (3)$$

where $q = \sqrt{-t}$ is the three-momentum transfer and the Pauli matrices $\boldsymbol{\sigma}$ are sandwiched between neutron and proton spinors. Here α is the spin-independent amplitude between the initial neutron and final proton, γ is a spin-orbit contribution, and β, δ, and ε are three spin-spin terms.

The orthogonal unit vectors used in eq. (3) are defined in terms of the initial neutron ($\boldsymbol{K}$) and final proton ($\boldsymbol{K'}$) cm momenta,

$$\boldsymbol{n} = \frac{\boldsymbol{K} \times \boldsymbol{K'}}{|\boldsymbol{K} \times \boldsymbol{K'}|}, \quad \boldsymbol{m} = \frac{\boldsymbol{K'} - \boldsymbol{K}}{|\boldsymbol{K'} - \boldsymbol{K}|}, \quad \boldsymbol{l} = \frac{\boldsymbol{K'} + \boldsymbol{K}}{|\boldsymbol{K'} + \boldsymbol{K}|}. \quad (4)$$

The amplitudes are normalised such that the $np \to pn$ differential cross section has the form

$$\left(\frac{\mathrm{d}\sigma}{\mathrm{d}t}\right)_{np\to pn} = |\alpha(q)|^2 + |\beta(q)|^2 + 2|\gamma(q)|^2 + |\delta(q)|^2 + |\varepsilon(q)|^2 \,. \quad (5)$$

In the ${}^1S_0$ limit of very low $E_{pp} = k^2/m_p$, where $\boldsymbol{k}$ is the pp relative momentum, the deuteron charge exchange necessarily involves a spin flip from the $S = 1$ of the deuteron to the $S = 0$ of the diproton. In this case the contribution from the spin-independent amplitude α drops out and one is left with only the spin-flip cross sections, as in the sum rule of eq. (2). The observables involving only the initial spins that are accessible at ANKE are linked to the amplitudes through [13,16]

$$\begin{aligned}
\frac{\mathrm{d}^4\sigma}{\mathrm{d}t\mathrm{d}^3k} &= \tfrac{1}{3} I \left\{ S^-(k, \tfrac{1}{2}q) \right\}^2 , \\
I\, A_y^d &= 0 \,, \\
I\, A_y^p &= -2\,\mathrm{Im}(\beta^*\gamma) \,, \\
I\, A_{xx} &= |\beta|^2 + |\gamma|^2 + |\varepsilon|^2 - 2|\delta|^2 R^2 \,, \\
I\, A_{yy} &= |\delta|^2 R^2 + |\varepsilon|^2 - 2|\beta|^2 - 2|\gamma|^2 \,, \\
I\, C_{y,y} &= -2\,\mathrm{Re}(\varepsilon^*\delta) R, \\
I\, C_{x,x} &= -2\,\mathrm{Re}(\varepsilon^*\beta), \\
C_{yy,y} &= -2A_y^p, \qquad (6)
\end{aligned}$$

where the spin-flip intensity

$$I = |\beta|^2 + |\gamma|^2 + |\varepsilon|^2 + |\delta|^2 R^2. \quad (7)$$

The function

$$R = S^+(k, \tfrac{1}{2}q) / S^-(k, \tfrac{1}{2}q) \quad (8)$$

is the ratio of two transition form factors that involve the S- and D-states of the deuteron wave function. In the forward direction $R = 1$.

Since $\gamma(q)$ vanishes in the forward direction, the contributions of $|\gamma(q)|^2$ to the cross section and the Cartesian tensor analysing powers A_{xx} and A_{yy} in eq. (6) are almost negligible under the conditions of the ANKE experiment. Measurements of the unpolarised cross section and the two transverse analysing powers can therefore determine separately the values of $|\beta(q)|^2$, $|\varepsilon(q)|^2$, and $|\delta(q)|^2$ at fixed momentum transfer q. The two deuteron-proton spin correlations that are measurable at ANKE, $C_{x,x}$ and $C_{y,y}$, fix two of the relative phases. The proton analysing power A_y^p gives mainly information on the spin-orbit amplitude $\gamma(q)$.

Although the formulae given here describe the general features of our data, detailed comparisons with theory are made using a program that takes higher final pp waves into account. These can, in particular, dilute the polarisation signals [13].

3 The experimental facility

The experiments reported here were carried out over three different time periods using the ANKE magnetic spectrometer [17] that is placed at an internal target position of the COoler SYnchrotron (COSY) [18] of the Forschungszentrum Jülich. Initially a polarised deuteron beam was used in conjunction with an unpolarised hydrogen cluster target [19]. In 2005 the $\vec{d}p \to \{pp\}_s n$ reaction was studied at deuteron beam energies $T_d = 1.2$, 1.6 and 1.8 GeV. The following year, the beam energy was increased to 2.27 GeV, with 1.2 GeV being repeated for polarimetry purposes. The equipment used was described in our earlier publications [12,14,15]. However, for the study of the spin-correlation parameters in 2009 [20], a newly developed polarised internal target [21–23] was installed at ANKE and this was employed in experiments at 1.2 and 2.27 GeV.

3.1 The polarised deuteron beam at COSY

The polarised deuterium ion source at COSY provides beams with different spin configuration [15]. It uses radio frequency transition units and quadrupole magnets to exchange the occupation numbers of the hyperfine states in the atom. The source was set up to provide a variety of states with different tensor and vector polarisations but, as listed in table 1, the selections differed for the experiments with cluster or polarised cell target.

The COSY cycles were configured to provide beam first at 1.2 GeV and then, without additional injection, accelerate the deuterons to one of the higher energies. This procedure allows the use of the polarisation export method [24], which is crucial in the measurement of spin observables at higher energies. This technique involves undertaking the polarimetry measurements at the lowest $T_d = 1.2$ GeV flat top energy, where the analysing powers are precisely known, and assuming that the beam polarisation is unchanged at the higher energy. This procedure is viable because there are no depolarising resonances for deuterons in the COSY energy range. This was checked at the 4% level by repeating the measurement of the analysing powers after deceleration [24].

3.2 The polarised hydrogen cell target at ANKE

The ANKE polarised internal gas target [23,25] uses an Atomic Beam Source (ABS) that is capable of producing

Table 1. The different configurations of the polarised deuteron ion source used in experiments carried out with the unpolarised cluster target, showing the nominal (ideal) values of the vector (P_z) and tensor (P_{zz}) polarisations and relative beam intensities. For the spin-correlation measurements, the more restricted set was used. Note, that P_z and P_{zz} are labeled conventionally in the reference frame of the source [15].

Experiment	State	I_0	P_z	P_{zz}
Unpolarised target	1	1	0	0
	2	1	$+\frac{1}{3}$	+1
	3	1	$-\frac{2}{3}$	0
	4	1	$+\frac{1}{3}$	−1
	5	1	$-\frac{1}{3}$	+1
	6	$\frac{2}{3}$	0	+1
	7	$\frac{2}{3}$	0	−2
	8	$\frac{2}{3}$	−1	+1
	9	$\frac{2}{3}$	+1	+1
Polarised target	1	1	0	0
	3	1	$-\frac{2}{3}$	0
	8	$\frac{2}{3}$	−1	+1

both polarised hydrogen and deuterium beams [26]. The first tests with the hydrogen atoms gave polarisations of $+0.89 \pm 0.01$ and -0.96 ± 0.01 for spin-up and spin-down, respectively [23,27].

The polarised atomic beam could be used directly from the source as a jet target. During the commissioning runs, the ABS demonstrated an integral jet-target thickness of about $1.5 \times 10^{11}\,\mathrm{cm}^{-2}$, which is consistent with the predicted value [27]. However, much higher target densities can be achieved if one uses a storage cell fed by the ABS. In order to achieve the maximum density, it is important to minimise the dimensions of the storage-cell tube. But, on the other hand, this limits the number of particles stored because of the beam heating and the consequent losses on the cell walls. A maximum target density of about $10^{13}\,\mathrm{cm}^{-2}$ was achieved with the cell during the commissioning runs and this resulted in luminosities of up to $10^{29}\,\mathrm{cm}^{-2}\mathrm{s}^{-1}$, depending upon the beam intensity [25].

During the 2009 beam time a cell made of 25 μm thick aluminium foil (99.95% Al) was used [21,22]. In order to minimise depolarisation on the cell surface, its inner walls were coated with Teflon. The cell had dimensions $X \times Y \times Z = 20 \times 15 \times 370\,\mathrm{mm}^3$, where Z is measured along the beam direction with X and Y referring to the horizontal and vertical transverse directions, respectively.

A dedicated beam development was required to ensure that the COSY beam passed successfully through the cell.

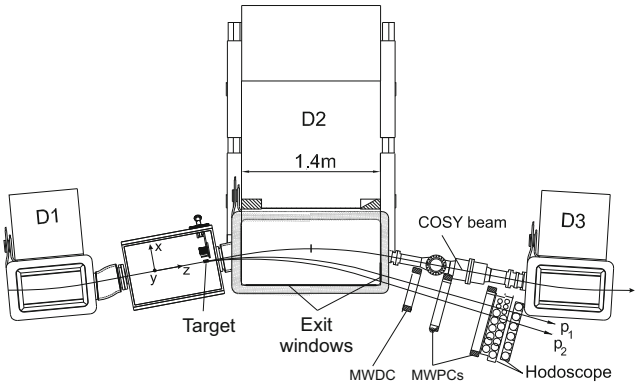

Fig. 1. The ANKE experimental set-up showing the positions of the three dipole magnets D1, D2, and D3. The Forward Detector (FD) consists of multiwire drift (MWDC) and multiwire proportional (MWPC) chambers, and a hodoscope composed of three layers of scintillation counters. For measurements with the polarised target, the ABS replaced the cluster-jet in the target chamber, with the detection system being identical in the two cases. The axes of the coordinate system are indicated.

Electron cooling [28] and stacking injection [29] were employed, with hundreds of injections per cycle to increase the number of stored deuterons in the beam. In order to avoid excessive background coming from the interactions of the beam halo particles with the cell wall, scrapers were installed upstream of the target region.

In the hydrogen case, the ABS was configured to produce two polarised states with equal gas densities. The polarisation of the hydrogen target was flipped between spin-up (↑) and spin-down (↓) every five seconds throughout the whole COSY cycle, which lasted for one hour. Such a procedure simplifies the later analyses by obviating the need to consider the luminosities while calculating the asymmetries between these states. In order to have a possibility to measure the target spin-up ↑ and spin-down ↓ polarisations separately, runs with an unpolarised hydrogen cell target were also undertaken.

3.3 The ANKE detection system

The forward detector system (FD) of the ANKE magnetic spectrometer, illustrated in fig. 1, is used for the deuteron charge-exchange studies. The multiwire chambers in the FD serve for track reconstruction and the three layers of the scintillation hodoscope permit the measurements of the arrival time and energy loss that are required for particle identification [30]. The main trigger used in the experiments consisted of a coincidence between the different layers in the hodoscope of the FD. To illustrate the acceptance of the apparatus for various final states, fig. 2 shows the experimental yield of ANKE for single charged particles at $T_d = 1.2\,\mathrm{GeV}$ in terms of the laboratory production angle in the horizontal plane and the magnetic rigidity. The kinematic curves for some of the possible nuclear reactions are also illustrated. Plots for the other beam energies are qualitatively similar.

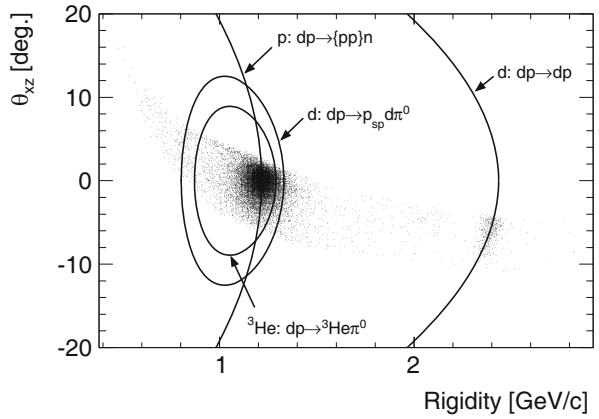

Fig. 2. Scatter plot of single charged particles detected in ANKE from the interaction of 1.2 GeV deuterons with a hydrogen cluster-jet target in terms of the laboratory production angle in the horizontal plane and the magnetic rigidity. The loci corresponding to four common nuclear reactions are also shown. These include the $dp \to \{pp\}_s n$ reaction at zero E_{pp}.

Among the reactions observed, there are two that are of particular interest, namely the deuteron charge-exchange $dp \to \{pp\}_s n$ and the quasi-free $dp \to p_{\rm sp} d\pi^0$, where the proton, $p_{\rm sp}$, has about half the beam momentum. The latter reaction is used to measure both the vector polarisation of the deuteron beam or hydrogen target and also the luminosity. After recording two charged particles, deuteron-proton pairs are separated from the remaining two-track events (mainly proton pairs) in the subsequent analysis by using the time information from the hodoscope. As demonstrated in fig. 3, if one assumes that both detected particles in the pair are protons, the calculated (ΔT_c) time of flight difference from the target does not match with the measured one (ΔT_m) for other pairs. One-dimensional projections of $\Delta T_m - \Delta T_c$ then show a consistent Gaussian peak corresponding to good pp final pairs. The background under the peak from other reactions is at least three orders of magnitude smaller, even at the highest beam energy. After recognising the two charged particles, the missing-mass distribution allows one to identify the reaction.

4 The cross section determination

The cross section σ for a given physical process is given in terms of the corresponding counting rate R and the luminosity L through

$$\sigma = R/L. \tag{9}$$

The luminosity, which is the product of the target density and beam intensity, can be measured in various ways. In the current analysis we relied on the measurement in parallel of the rate for a process with a well-known and sizeable cross section. Once the luminosity is known, absolute values of cross sections for other reactions can be deduced from the count rates measured in the experiment.

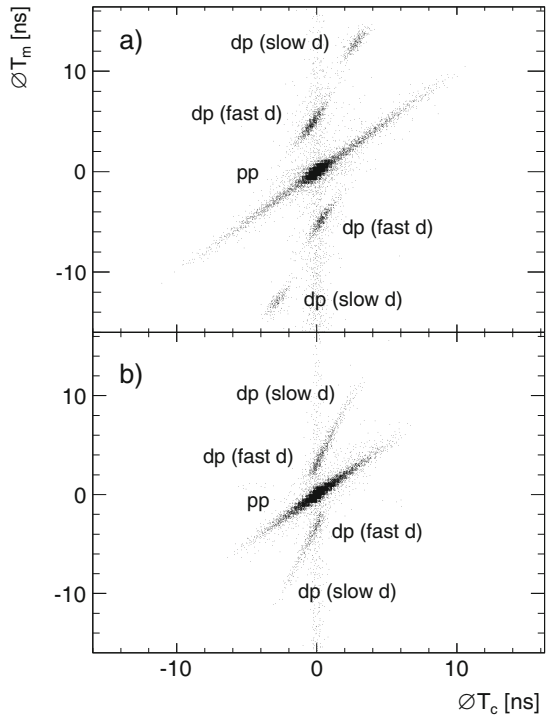

Fig. 3. Scatter plot of measured (ΔT_m) and calculated (ΔT_c) time differences between pairs of charged particle registered in the ANKE forward detector at a) $T_d = 1.2$ GeV and b) $T_d = 2.27$ GeV. ΔT_c was calculated assuming that both particles were protons. The separation between dp and pp pairs is very clear.

4.1 The $dp \to p_{\rm sp} d\pi^0$ reaction

The $dp \to p_{\rm sp} d\pi^0$ reaction is used in the determination of the luminosity in this experiment. This is identified in the ANKE forward detector by detecting both charged particles (cf. figs. 2 and 3). After recognising the dp-pairs, the reaction is finally isolated on the basis of the missing-mass distributions [12]. There is an accidental background at very small $|\Delta T_c|$ that is randomly distributed in ΔT_m. This is caused by fast particles, mainly protons, that are produced in a different beam-target interaction. The contribution from such accidental events in the vicinity of the fast deuteron branch of the $dp \to p_{\rm sp} d\pi^0$ reaction increases rapidly with energy. It varies between 18% and 30% for $T_d \geq 1.6$ GeV, whereas it is less then 3% at 1.2 GeV. The background is negligible at all energies for the slow deuteron branch.

The properties of background were studied using the data for which $|\Delta T_c| < 2$ ns and $|\Delta T_m| > 12$ ns. As can be seen from fig. 3, no true coincidence two-track events are expected in this region. These data provided the shape of background in the distributions of the missing mass and the deuteron laboratory scattering angle in the $dp \to p_{\rm sp} d\pi^0$ reaction. The normalisation for the background was found by comparing the background missing-mass spectra with that for the identified dp pairs. The normalised background was then subtracted from the $dp \to p_{\rm sp} d\pi^0$ angular distributions.

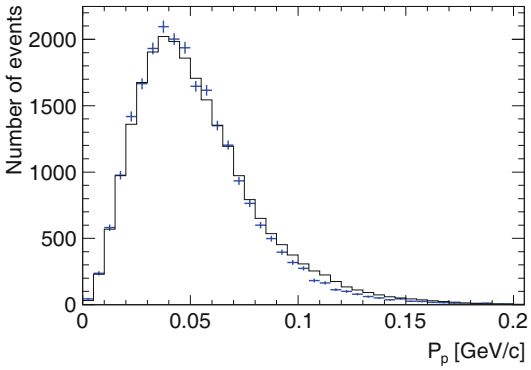

Fig. 4. The momentum distribution of the fast proton from the $dp \to p_{\rm sp}d\pi^0$ reaction at $T_d = 1.2\,\text{GeV}$, transformed into the rest frame of the incident deuteron is compared with the Monte Carlo simulation (solid histogram).

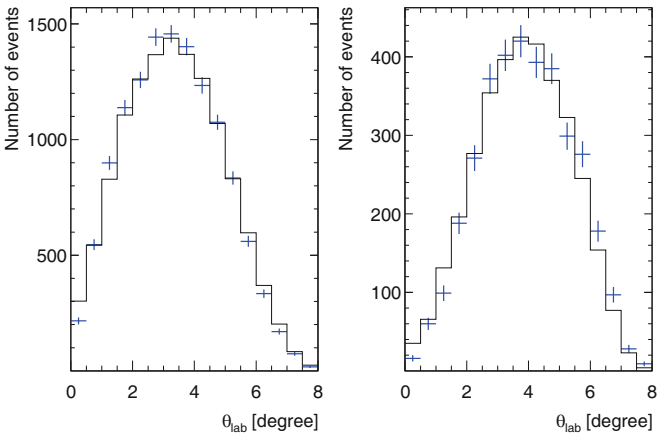

Fig. 5. Simulated (solid histogram) and experimental angular distributions for the $dp \to p_{\rm sp}d\pi^0$ reaction at $T_d = 1.2\,\text{GeV}$. The left and right panels correspond to fast and slow deuterons, respectively.

At intermediate energies, soft deuteron collisions are generally dominated by the interaction of one of the nucleons in the nucleus, the other nucleon being a spectator. When the proton acts as a spectator, $p_{\rm sp}$, the $dp \to p_{\rm sp}d\pi^0$ reaction can be interpreted in terms of quasi-free $np \to d\pi^0$ pion production. To confirm the spectator hypothesis, a Monte Carlo simulation has been performed within PLUTO [31] using the Fermi momentum distribution from the Paris deuteron wave function [32]. As is clear from fig. 4, the data are consistent with quasi-free production on the neutron leading to a spectator proton. However, in order to reduce further possible contributions from multiple scattering and other mechanisms, only events below $60\,\text{MeV}/c$ were retained for the luminosity evaluation.

The determination of the angles for the quasi-free $np \to d\pi^0$ reaction is complicated by the Fermi motion of the nucleons inside the deuteron. Due to this effect, the effective neutron beam energy, T_n, is spread around half the deuteron beam energy with a width arising from the Fermi momentum. At a beam energy of 600 MeV per nucleon, the FWHM is 90 MeV for a $p_{\rm sp} < 60\,\text{MeV}/c$ cut. Furthermore, the neutron direction is not precisely aligned along that of the beam, but is spread over some solid angle. Since this introduces an incident angle, which is several degrees in the laboratory system (depending on the beam energy), it has to be taken into account. These considerations apply to both the polar and azimuthal angles. In order to correct for this effect, the three-momentum of the incident neutron was reconstructed using the information from the spectator-proton momentum. The deuteron polar angle was measured from the neutron momentum instead of the beam direction. The azimuthal angle was defined between the normals to the COSY ring and deuteron scattering plane.

Isospin invariance requires the cross section for $np \to d\pi^0$ to be half of that for $pp \to d\pi^+$, for which there are numerous measurements [33]. An additional advantage of using this reaction for normalisation is that the typical 5% shadowing effect in the deuteron (where one nucleon hides behind the other) should be broadly similar in the $dp \to \{pp\}X$ and $dp \to p_{\rm sp}d\pi^0$ reactions.

In order to investigate the acceptance of the ANKE forward detector for different reactions, a full simulation was performed based on GEANT software [34]. The same track reconstruction algorithm was used in the simulation and the data analysis. In order to get as precise a description of the experiment as possible, the dispersion of the hits in the MWPC, the background hits produced by accidental coincidences, and the noise in the multiwire chambers readout electronics, as obtained from the experimental data, were also included in the simulation [30]. The quality of the simulation may be judged from the distributions of the deuteron production angle in the laboratory system that are shown in fig. 5.

4.2 Luminosity measurements

To determine the luminosity we use eq. (9) and insert detailed expressions for R and σ,

$$L = \frac{R}{\sigma} = \frac{R_{\rm exp}\,(N_{\rm tot}/N_{\rm acc})}{\iint \frac{\mathrm{d}\sigma}{\mathrm{d}\vartheta}(\vartheta, T_n)\,\mathrm{d}\vartheta\,\mathrm{d}T_n}, \tag{10}$$

where $R_{\rm exp}$ is the count rate from the quasi-free $np \to d\pi^0$ reaction, corrected for the trigger dead time. $N_{\rm acc}$ is the number of counts in the simulation that pass all the criteria used in the experimental data processing and $N_{\rm tot}$ is the total number of simulated events. These are summed over the neutron kinetic energy, subject to the $p_{\rm sp} < 60\,\text{MeV}/c$ cut, and over the given angular range. The $\mathrm{d}\sigma(\vartheta, T_n)/\mathrm{d}\vartheta$ differential cross section was taken from the $pp \to d\pi^+$ database [33], where ϑ is the deuteron polar angle in the laboratory frame.

The FD detector acceptance changes rapidly with angle. In order to minimise systematic errors, the total angular range was binned and the luminosity evaluated separately for each bin. Data at the acceptance edges (the smallest and the largest angles) were less reliable, due to the greater uncertainty in the evaluation of the

Table 2. Average luminosities achieved with the cluster-jet target at four different beam energies. Shown separately are the uncertainties associated with the measurement and with the experimental data used as input in the estimations.

T_d	Average luminosity	Measurement uncertainty	SAID uncertainty
[GeV]	[$\mathrm{cm^{-2}s^{-1}}$]	[%]	[%]
1.2	1.76×10^{30}	1.1	2.2
1.6	1.84×10^{31}	2.0	5.1
1.8	1.61×10^{31}	2.8	4.4
2.27	1.18×10^{30}	5.0	3.8

acceptance, and showed systematic shifts in luminosity. Such angular intervals were discarded and the average recomputed.

The values of the average luminosities determined from the $np \rightarrow d\pi^0$ reaction are given in table 2. The errors quoted include statistical ones from the experimental counts and those introduced by the background subtraction procedure. Uncertainties coming from the SAID database [33], which were estimated by studying the experimental results in the relevant regions, are listed separately.

4.3 The dp → {pp}$_s$n cross section

Having identified two fast protons in the final state and selected low E_{pp} events, the $dp \rightarrow \{pp\}_s n$ reaction was isolated on the basis of the missing-mass distributions, which are shown at three energies in fig. 6. In addition to the dominant neutron peak, there are also many events for $M_x > 1080\,\mathrm{MeV}/c^2$ that must correspond to pion production [35]. However, very few of these leak into the neutron region and the background from this under the neutron peak is at most at the per cent level. This is also true for data in the individual momentum-transfer q bins. Random background, which was studied using the timing information, was at the 1–3% level and could be easily subtracted.

The $dp \rightarrow \{pp\}_s n$ cross section determination was performed in a similar manner to the luminosity evaluation that used the $dp \rightarrow p_{\mathrm{sp}} d\pi^0$ reaction. It involved the same technique for correcting the experimental count rates and estimating the detector acceptance. Since the $dp \rightarrow \{pp\}_s n$ reaction has a three-body final state, in principle the cross section is a function of five independent variables. However, within the impulse approximation, by far the most important of these for very low E_{pp} are the excitation energy E_{pp} in the final pp diproton and the momentum transfer q from the proton to the neutron. In accordance with eq. (9), the two-dimensional differential cross section was evaluated in terms of the integrated luminosity L_{int} from

$$\frac{\mathrm{d}^2\sigma(q, E_{pp})}{\mathrm{d}q\,\mathrm{d}E_{pp}} = \frac{1}{L_{\mathrm{int}}} \frac{N_{\mathrm{exp}}(q, E_{pp})\, N_{\mathrm{tot}}(q, E_{pp})}{N_{\mathrm{acc}}(q, E_{pp})\, \Delta q\, \Delta E_{pp}}, \qquad (11)$$

where $N_{\mathrm{exp}}(q, E_{pp})$ is the corrected number of experimental events for given values of q, measured in laboratory system, and E_{pp}. $N_{\mathrm{tot}}(q, E_{pp})$ and $N_{\mathrm{acc}}(q, E_{pp})$ are the total and accepted numbers of simulated events, respectively. Δq and ΔE_{pp} correspond to bin widths in momentum transfer and excitation energy, respectively. The resolutions in q and E_{pp} are about 4–8 MeV/c and better than 0.3 MeV, respectively.

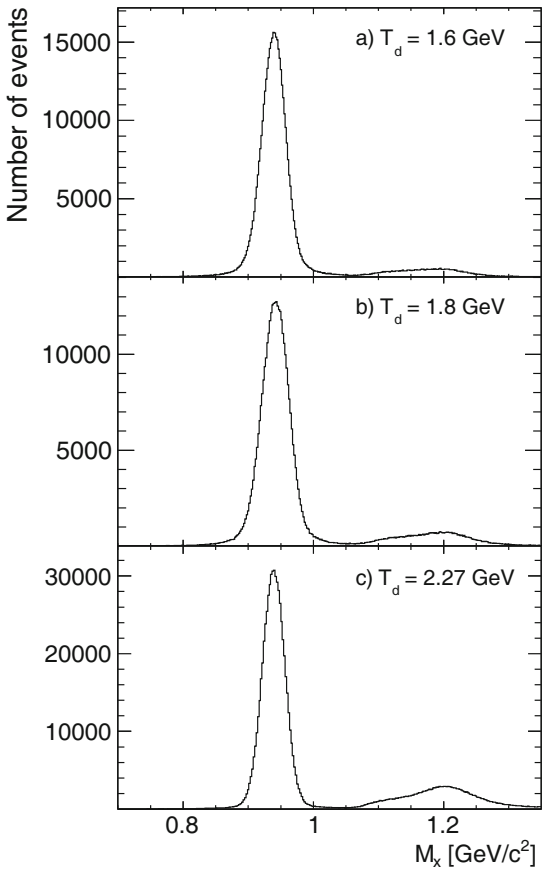

Fig. 6. The missing-mass M_x distributions for the $dp \rightarrow \{pp\}_s X$ reaction at three deuteron beam energies. The background under the neutron peak is a negligible.

The cross sections were further integrated over $E_{pp} < 3$ MeV in order to provide the $\mathrm{d}\sigma/\mathrm{d}q$ differential distribution presented in fig. 7. This includes also the new results obtained at $T_d = 1.2$ GeV. In addition to the statistical errors arising from the experimental count rates that are shown, there are also overall systematic uncertainties arising from the luminosity determinations, given in table 2. Within these uncertainties, the agreement with the theoretical impulse approximation predictions [13] at $T_d = 1.2$, 1.6, and 1.8 GeV is very encouraging and is in line with similar data analysed at 1.17 GeV [12]. In contrast, the unpolarised differential cross section at $T_d = 2.27$ GeV falls about 15% below the predictions based upon the cur-

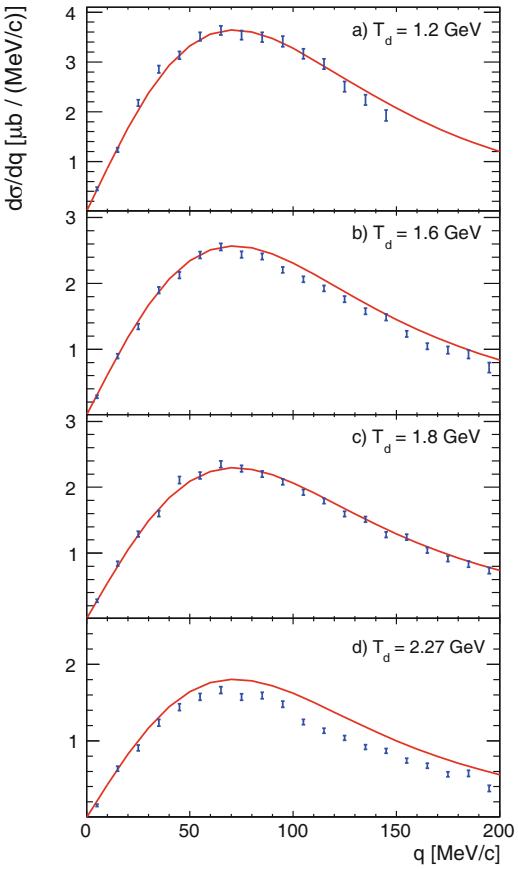

Fig. 7. Differential cross sections for the $dp \to \{pp\}_s n$ reaction at four different energies compared with impulse approximation predictions based upon the current SAID $np \to np$ amplitude analysis [1]. The data are integrated over the $E_{pp} < 3$ MeV interval. Only statistical errors are shown. Systematic uncertainties are listed in table 2.

rent $np \to np$ partial wave analysis [1]. As we shall see later, similar discrepancies are found in the spin observables of the $dp \to \{pp\}_s n$ reaction but only at this highest energy.

5 Determination of deuteron analysing powers

In order to measure the deuteron analysing powers for the $\vec{d}p \to \{pp\}_s n$ or other reaction, the first step has to be the identification of the polarisations of the various deuteron beams used in the experiment. With complete efficiencies in the transition units, the polarisations should approach the ideal values given in table 1. However, this is never the case in practice and the beam polarisation must be determined separately for each of the beams used. In our earlier work at 1.17 GeV [12], a variety of nuclear reactions with known analysing powers were measured and these were used to establish values for the polarisations. These showed that the analysing powers for the $\vec{d}p \to \{pp\}_s n$ reaction were well reproduced in the impulse approximation calculations [13]. Since the deuteron charge-exchange reaction can be so well identified and measured at ANKE, we use this reaction itself to measure the beam tensor polarisation at the neighbouring energy of 1.2 GeV, the necessary analysing powers being taken from the impulse approximation estimates. Apart from the large counting rates, this approach has the advantage of being insensitive to the deuteron vector polarisation. By comparing the predictions of the current and SP96 SAID solutions [1], differences of less than 4% are found in the extracted values of P_{zz} at 600 MeV. This is consistent with the typical 5% uncertainty quoted in ref. [12].

5.1 Tensor polarisation of the deuteron beam

The tensor polarisation of the deuteron beam was measured using the $dp \to \{pp\}_s n$ reaction at $T_d = 1.2$ GeV. The circulating deuteron beam was polarised perpendicularly to the horizontal plane of the machine. As already mentioned, the beam vector (P_z) and tensor (P_{zz}) polarisations are labeled conventionally in the reference frame of the source. In contrast, all the spin observables discussed later refer to the right-handed coordinate system of the reaction frame, where the beam defines the Z-direction while the stable spin axis of the beam points along the Y-direction, which is perpendicular to the COSY orbit.

No dependence is expected on the vector polarisation for small E_{pp} [7] and this was checked in our earlier experiment [12]. The numbers $N(q, \phi)$ of diprotons produced at momentum transfer q and azimuthal angle ϕ with respect to the X-direction are given in terms of the beam polarisation by

$$\frac{N(q,\phi)}{N_0(q)} = C_n \left\{1 + \tfrac{1}{4} P_{zz} \left[A_{xx}(q)(1 - \cos 2\phi) + A_{yy}(q)(1 + \cos 2\phi)\right]\right\}, \quad (12)$$

where $N_0(q)$ are the numbers for an unpolarised beam and C_n is the relative luminosity of the polarised beam.

During the course of the polarised measurements, various configurations of the ion source were used and the beam polarisation had to be determined separately for each state. Several methods to fix the relative luminosities C_n of a state with respect to the unpolarised mode are possible at ANKE [24]. The one provided by the $dp \to p_{\rm sp} X$ reaction is preferable because the number of single-track events is enormous for all beam energies. No dependence of the rates on the tensor polarisation of the deuteron beam was found for proton spectator momenta below 60 MeV/c.

The break-up data were divided into several bins of momentum transfer q and distributions in $\cos 2\phi$ were constructed for each bin and polarisation mode. The ratios to the unpolarised state were fitted using eq. (12), the theoretical predictions for A_{xx} and A_{yy} being taken at mean values of q in each bin. The validity of this approach was checked at $T_d = 1.17$ GeV in the earlier experimental studies at ANKE [14]. The beam polarisation in each state was taken as the weighted average over the different values of the momentum transfer.

The maximum values of P_{zz} were $\approx 85\%$ of the ideal values for the 2005 data. But, in the 2006 data, the maximum tensor polarisation dropped to $\approx 55\%$ of the ideal, with little change in the vector polarisation. The difference has been ascribed to the changed efficiencies of the units in the COSY deuterium ion source [24]. For the high $|P_{zz}|$ modes in table 1, the estimated polarisation varied in the (0.75–0.85) range in the 2005 data and in the (0.39–0.60) range in the 2006 data. The typical uncertainty in P_{zz} was 0.02–0.04.

The vector analysing power of the $\vec{d}p \to \{pp\}_s n$ reaction is predicted to vanish in the $^1S_0$ limit [7] and this was confirmed at 1.17 GeV in our earlier work [12]. As a consequence, the vector polarisation of the beam is unimportant for the tensor analysing power studies carried out with the cluster target. This is no longer the case for the spin-correlation measurements with the polarised cell target. The determination of the vector polarisation of the deuteron beam in this case is described in sect. 6.

5.2 Deuteron tensor analysing powers

The deuteron Cartesian tensor analysing powers A_{xx} and A_{yy} were extracted using eq. (12) in much the same way as for the polarimetry, with the beam tensor polarisation P_{zz} being determined at $T_d = 1.2$ GeV. The ratios of the polarised to unpolarised corrected count rates were fitted in terms of the two free parameters A_{xx} and A_{yy}. The procedure was repeated for different polarisation states and results averaged over these source modes.

The results for the tensor analysing powers are shown in fig. 8 at three beam energies as functions of the momentum transfer. The agreement between the experimental data and the impulse approximation predictions is very good at $T_n = 800$ and 900 MeV. At these energies the SAID np amplitudes [1] used as input in the calculations are considered to be reliable but at 2.27 GeV, the maximum deuteron energy available at COSY, the agreement is much worse. Since there are also severe discrepancies in the unpolarised cross section at this energy, it is natural to question whether there might be deficiencies in the SAID np analysis at this energy.

The experimental value of $A_{xx} = A_{yy}$ in the forward direction ($q \approx 0$) is significantly more negative than the predictions using the SAID np amplitudes at 1.135 GeV. However, it can be seen from eq. (6) that a relative reduction in the ε amplitude might improve the predictions. To check this possibility, the predictions were recomputed with the $\varepsilon(q)$ amplitude being reduced uniformly by 25%. This gives the much better overall agreement with the data that is demonstrated by the dashed curves in the lower panel of fig. 8. This therefore suggests that the current SAID amplitudes [1] might overestimate the relative strength of the $\varepsilon(q)$ at small q but further proof is required and this is furnished by the measurements of the spin correlations.

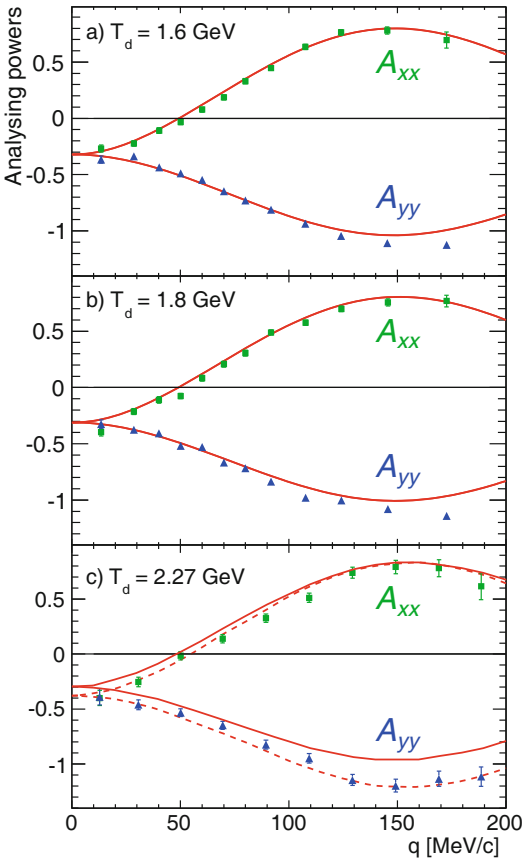

Fig. 8. Tensor analysing powers A_{xx} (squares) and A_{yy} (triangles) of the $\vec{d}p \to \{pp\}_s n$ reaction at three beam energies for low diproton excitation energy, $E_{pp} < 3$ MeV, compared to impulse approximation predictions based upon the current SAID $np \to np$ amplitudes [1]. The dashed curves at 2.27 GeV correspond to a uniform reduction of the spin-longitudinal $\varepsilon(q)$ amplitude by 25%. The error bars include the uncertainties from the relative luminosity C_n and the beam polarisations determined at 1.2 GeV [24]. In addition, at the higher energies there is an overall uncertainty of up to 4% due to the use of the polarisation export procedure.

6 Determination of the deuteron-proton spin-correlation parameters

In experiments with the unpolarised cluster-jet target, the $\vec{d}p \to \{pp\}_s n$ reaction is only sensitive to the tensor polarisation of the beam and the values of this could be established by using the $\vec{d}p \to \{pp\}_s n$ reaction itself at the 1.2 GeV calibration energy, as described in sect. 5. In contrast, in order to determine the spin-correlation parameters $C_{x,x}$ and $C_{y,y}$, one has first to determine the vector polarisation of the deuteron beam as well as the polarisation of the hydrogen in the target cell. The basis of both measurements is the quasi-free $\vec{n}p \to d\pi^0$ reaction which, at small spectator momenta, is insensitive to the deuteron tensor polarisation.

6.1 The beam and target polarimetry

The polarisation of the hydrogen target and the vector polarisation of the deuteron beam were both determined using the quasi-free $np \to d\pi^0$ reaction. Now it is well known that, if one integrates over all Fermi momenta inside the deuteron, the nucleon polarisation in the deuteron P_z^n would be reduced from that of the deuteron P_z^d by a factor

$$P_z^n = \left(1 - \tfrac{3}{2} P_D\right) P_z^d, \qquad (13)$$

where P_D is the deuteron D-state probability. However, since the D-state effects vanish like $(p_{\rm sp})^2$, the dilution of the polarisation signal by the deuteron D-state is negligible if only data with $p_{\rm sp} < 60\,{\rm MeV}/c$ are used in the subsequent analyses. Such a cut preserves a large part of the statistics.

For an unpolarised deuteron beam incident on a polarised hydrogen target with spin-up ($\uparrow$) and spin-down ($\downarrow$), the asymmetry ratio ϵ between polarised $N^{\uparrow(\downarrow)}$ and unpolarised N^0 yields has the form

$$\epsilon^{\uparrow(\downarrow)}(\theta,\phi) = \frac{N^{\uparrow(\downarrow)}(\theta,\phi)}{N^0(\theta)} = 1 + Q^{\uparrow(\downarrow)} A_y(\theta)\cos\phi, \qquad (14)$$

where θ and ϕ angles are polar and azimuthal angles, respectively, of the detected particle and Q is the target polarisation. The polar ϑ and azimuthal ϕ angles of the deuteron were determined according to the procedure described in sect. 4.1.

Isospin invariance requires the analysing powers in the $np \to d\pi^0$ and $pp \to d\pi^+$ reactions to be identical and there are numerous measurements of the proton analysing power $A_y(\theta)$ of the latter in the 600 MeV region [33]. The dispersion of the results introduces a $\approx 2.3\%$ uncertainty in the value of the polarisation and, since the relevant angular domains are different for the beam and target determinations, these are largely independent for P and Q.

6.2 The dp $\to$ p$_{sp}$dπ^0 reaction with the cell target

The cell introduces additional complications in the determination of the angles because of the spread of the interaction points along the cell axis. The reconstruction of the longitudinal vertex coordinate Z is therefore required for each event. For a two-track event, this can be done with the use of the arrival time difference for two particles, measured in the scintillation hodoscope. In our kinematical conditions, where the deuteron is at least twice as slow as the proton, such a difference is a sensitive function of Z. The three-momenta of the two particles and the Y and Z coordinates of the vertex are found through an overall fit procedure that uses the information from both the wire chambers and the hodoscope.

Figure 9 shows the distribution of interaction points in the Y-Z plane. In addition to helping in the angular determination, the vertex reconstruction allows one to make cuts along the cell axis to minimise the background from the rest gas that is spread throughout the target chamber.

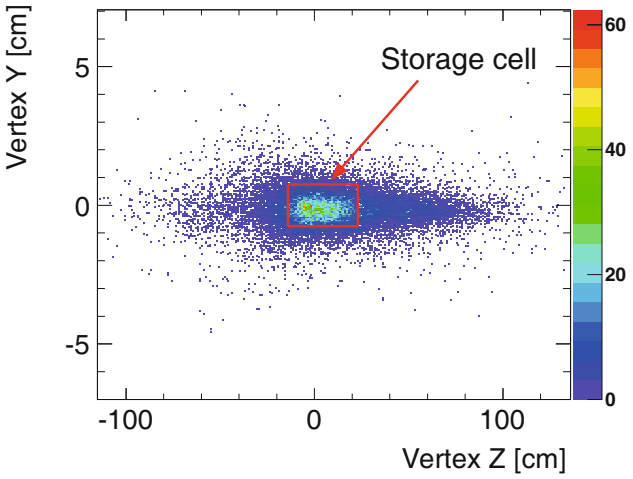

Fig. 9. Vertex reconstruction in the YZ plane using correlated deuteron-proton pairs. The rectangle shows the physical dimensions of the cell ($Y \times Z = 15 \times 370\,{\rm mm}^2$).

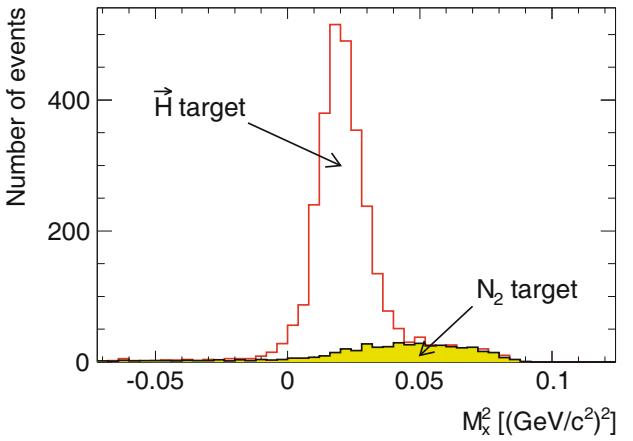

Fig. 10. Comparison of the $(d, dp_{\rm sp})$ missing-mass–squared distributions at $T_d = 1.2\,{\rm GeV}$ when using a polarised hydrogen target or filling the cell with nitrogen gas.

A second major complication arises from the scattering of the beam halo particles on the cell walls. This can produce additional background that would dilute the analysing power signal. As mentioned earlier, the dedicated beam development enabled the bulk of the beam to pass through the cell without hitting the walls. For this reason, recording data with an empty cell would take much more time to collect sufficient statistics to determine the background. Additional runs were therefore recorded where nitrogen gas was injected into the cell to simulate the shape of the background (see details in refs. [21,22]). The background subtraction was performed for each polarisation state by using the missing-mass distributions for the hydrogen and nitrogen data. One such example is shown in fig. 10.

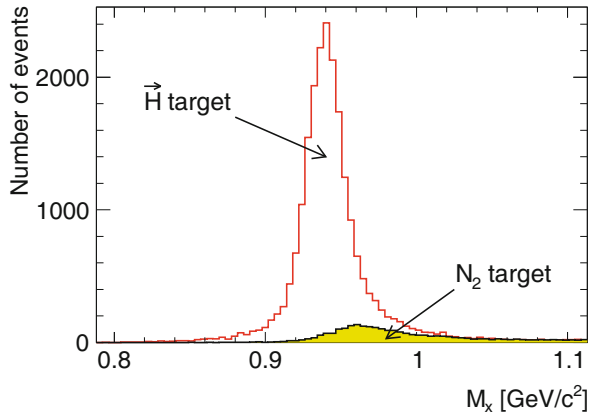

Fig. 11. Comparison of the (d, pp) missing-mass distributions at $T_d = 1.2$ GeV beam energy when using a polarised hydrogen target or filling the cell with nitrogen gas.

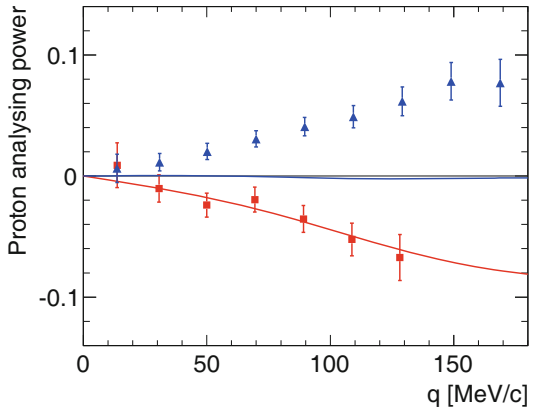

Fig. 12. Proton analysing powers A_y^p for the $dp \to \{pp\}_s n$ reaction at $T_d = 1.2$ (red squares) and 2.27 GeV (blue triangles) for $E_{pp} < 3$ MeV. The error bars do not include the 5% uncertainties arising from the target polarisation. Curves correspond to the theoretical predictions. Note that at 2.27 GeV the A_y^p prediction is very small and hardly visible on this scale.

6.3 The target and beam polarisation

The target polarisation was measured using data taken with an unpolarised deuteron beam at $T_d = 1.2$ GeV. After vertex reconstruction, the $np \to d\pi^0$ data were binned in deuteron cm angles. The background subtraction was performed separately for each bin and distributions in $\cos\phi$ built for both spin-up and spin-down modes. The weighted sum of the two data sets from different target polarisations was taken as the unpolarised mode. Weights were determined according to the relative asymmetries with respect to the unpolarised state. The ratios of the difference to the sum of the data for the two polarised modes were than fitted with a linear function in $\cos\phi$ and the value of the product QA_y deduced. Taking the mean analysing power $\langle A_y \rangle$ in each θ_d^{cm} bin from the SAID $pp \to d\pi^+$ database [33], this gave $Q^\uparrow = 0.61 \pm 0.02$ and $Q^\downarrow = -0.70 \pm 0.03$.

Using the quasi-free $np \to d\pi^0$ reaction, in an analogous way to that for the target polarisation, the vector polarisation of the deuteron beam (state 3 in table 1), was determined to be $P_z = -0.51 \pm 0.05$.

6.4 Measurement of the deuteron-proton spin-correlation parameters

The double-polarised experimental data from the 2009 beam time offers an excellent opportunity for studies of the spin-correlation parameters $C_{x,x}$ and $C_{y,y}$ to determine the relative phases of the spin-spin amplitudes [20]. Furthermore, it is of interest to see whether the suspected ε deficiencies in the SAID amplitudes at highest beam energy are reflected also in the spin correlations.

The background subtraction was carried out in the same way as for the $dp \to d\pi^0 p_{\rm sp}$ reaction, with the nitrogen gas data simulating the shape of the background, as illustrated in fig. 11.

In order to extract the spin-correlation parameters from the $\vec{d}\vec{p} \to \{pp\}_s n$ reaction, no tensor polarised deuteron beam modes were used (see table 1). In this case the ratio of the polarised $N(q, \phi)$ to unpolarised $N^0(q)$ yields has the form [36]

$$\frac{N(q,\phi)}{N^0(q)} = 1 + QA_y^p(q)\cos\phi + \tfrac{3}{2}P_z A_y^d(q)\cos\phi + \tfrac{3}{4}P_z Q[(1+\cos 2\phi)C_{y,y}(q) + (1-\cos 2\phi)C_{x,x}(q)]. \quad (15)$$

Although the experiment was designed for the study of spin correlations, by analysing first the polarised target yields for an unpolarised deuteron beam, we could obtain the dependence of the target analysing power A_y^p on q that is presented in fig. 12 at 1.2 and 2.27 GeV. This is predicted very well in impulse approximation at the lower energy but at 2.27 GeV the corresponding prediction can hardly be distinguished from the x-axis on this scale. Equation (6) then suggests that there must be a serious problem also with the SAID determination of the spin-orbit amplitude $\gamma(q)$ at 1.135 GeV.

In impulse approximation A_y^d vanishes [7], which is consistent with our measurements at 1.17 GeV [12], and this simplifies the determination of $C_{x,x}$ and $C_{y,y}$ using data with polarised beam and polarised target. After binning the normalised counts in intervals in q, the $\cos 2\phi$ dependence in eq. (15) allowed us to extract the $C_{x,x}$ and $C_{y,y}$ coefficients separately. Note, that the resolutions in both E_{pp} and q in the cell target data are similar to those achieved with the cluster target.

The spin-correlation data for an $E_{pp} < 3$ MeV cut are compared with theoretical predictions in fig. 13. The good agreement with the experimental points at $T_d = 1.2$ GeV shows that the two relative phases between the spin-spin amplitudes are well predicted by the SAID program at this energy. It can, however, not come as a complete surprise to

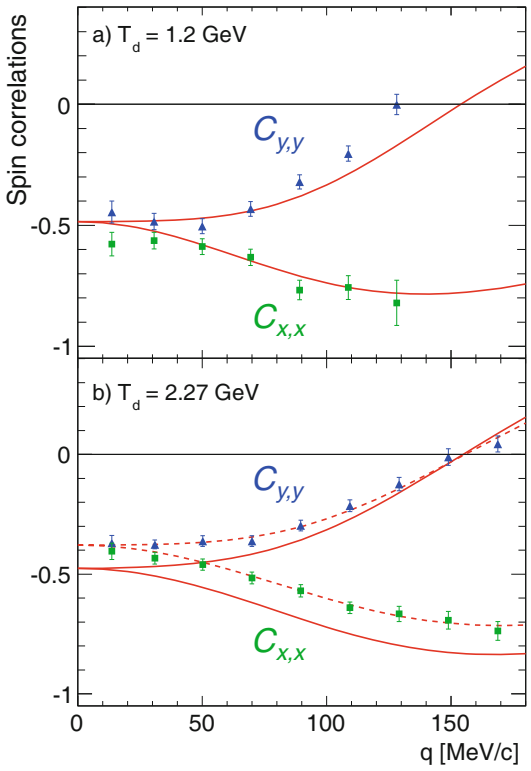

Fig. 13. The spin-correlation coefficients $C_{x,x}$ and $C_{y,y}$ for the $dp \to \{pp\}_s n$ reaction at $T_d = 1.2$ and 2.27 GeV for $E_{pp} < 3$ MeV. The error bars do not include the 11% uncertainties in the combined beam and target polarisations. The curves are impulse approximation predictions; dashed curves at 2.27 GeV correspond to $|\varepsilon(q)|$ being reduced by 25%.

find that there are serious discrepancies at $T_d = 2.27$ GeV but, as shown by the dashed line, these largely disappear if the SAID $\varepsilon(q)$ amplitude is scaled uniformly by a factor of 0.75, *i.e.*, by the same factor that brought agreement for the A_{xx} and A_{yy} observables!

7 Conclusions and outlook

We have measured the unpolarised differential cross section and the Cartesian tensor analysing powers in the $\vec{d}p \to \{pp\}_s n$ reaction for small momentum transfers between the proton and neutron by using a hydrogen cluster target in combination with a tensor polarised deuteron beam. The cross section data at 1.2, 1.6, and 1.8 GeV are very well described in impulse approximation using the current SAID solution for the np amplitudes. These amplitudes suffer from much bigger ambiguities at higher energies and the corresponding cross section prediction is about 15% too high compared to our results at 2.27 GeV, though one must bear in mind the 6% uncertainty in the overall normalisation of the data at this energy. The suspicion must fall on the SAID solution, which predicts an unpolarised $np \to pn$ cross section that may be up to 10% too large [2], of which the spin-dependent contribution is also about 10% too large [5].

The description of A_{xx} and A_{yy} is also very good at the three lower energies but much poorer at 2.27 GeV. Since one would expect the impulse approximation to become better as the energy is raised, attention is once again focussed on the SAID np amplitudes. The strength of $|\varepsilon(0)|^2$ in np charge exchange relative to $|\beta(0)|^2 = |\delta(0)|^2$ is determined by the spin-transfer parameters $K_{LL}(0)$ and $K_{NN}(0)$, but there are no measurements of these quantities in the relevant angular and energy region. This limits severely the SAID predictive power for the deuteron tensor analysing powers. To fit our data, we have reduced the SAID prediction for $\varepsilon(q)$ uniformly by 25% and this reproduces the results much better. Although this might be improved further by introducing a q-dependence in this factor, the present data do not justify such a refinement.

By replacing the unpolarised hydrogen cluster-jet target by a polarised hydrogen gas cell, it was possible to measure the spin-correlation coefficients $C_{x,x}$ and $C_{y,y}$ in the $\vec{d}\vec{p} \to \{pp\}_s n$ reaction with a vector polarised deuteron beam, but only at 1.2 and 2.27 GeV. The behaviour seen here is similar to that for the other observables, with a good description being achieved at 1.2 GeV whereas at 2.27 GeV a reduction of the order of 25% seems to be required in the ε input.

As a by-product of the polarised cell experiment, we were also able to measure the proton analysing power in the reaction. As with the other observables, impulse approximation reproduces well the small A_y^p signal at 1.2 GeV but fails completely at 2.27 GeV. This suggests that the SAID solution for the γ-amplitude is also unreliable at the higher energy.

In summary, the fact that the impulse approximation with the current SAID input reproduces well all our data below 1 GeV per nucleon gives us confidence that the charge-exchange methodology works well. However, the discrepancies seen at the higher energy can only be resolved by reducing the strength of the spin-spin amplitudes, especially in the longitudinal direction, while increasing the spin-orbit contribution. It is therefore evident that the charge exchange on the deuteron contains valuable information on the neutron-proton amplitudes. The challenge is to get this used inside the SAID program.

The experiments reported here were carried out up to the maximum deuteron energy available at COSY. To go higher in energy at this facility, an experiment would have to be undertaken in inverse kinematics with a polarised proton incident on a polarised deuterium gas cell [21,22], with the two slow protons being detected in the Silicon Tracking Telescopes [37]. This will allow the studies reported here to be continued up to 2.9 GeV per nucleon [11,38].

We are grateful to the accelerator crew for the reliable operation of COSY and the deuteron polarimeters. We would like to thank I.I. Strakovsky for many useful discussions and for providing us with values of the current SAID neutron-proton amplitudes. The work was supported by the COSY FFE programme and the Shota Rustaveli National Science Foundation Grant 09-1024-4-200.

References

1. R.A. Arndt, I.I. Strakovsky, R.L. Workman, Phys. Rev. C **62**, 034005 (2000) `http://gwdac.phys.gwu.edu`.
2. G. Bizard *et al.*, Nucl. Phys. B **85**, 14 (1975).
3. N.W. Dean, Phys. Rev. D **5**, 1661 (1972).
4. N.W. Dean, Phys. Rev. D **5**, 2832 (1972).
5. V.I. Sharov *et al.*, Eur. Phys. J. A **39**, 267 (2009).
6. F. Lehar, C. Wilkin, Phys. Part. Nucl. Lett. **7**, 235 (2010).
7. D.V. Bugg, C. Wilkin, Nucl. Phys. A **467**, 575 (1987).
8. I.Ya. Pomeranchuk, Dokl. Akad. Nauk. USSR **78**, 249 (1951).
9. C. Ellegaard *et al.*, Phys. Rev. Lett. **59**, 974 (1987).
10. S. Kox *et al.*, Nucl. Phys. A **556**, 621 (1993).
11. A. Kacharava, F. Rathmann, C. Wilkin, *Spin Physics from COSY to FAIR*, COSY proposal **152** (2005) arXiv:nucl-ex/0511028.
12. D. Chiladze *et al.*, Eur. Phys. J. A **40**, 23 (2009).
13. J. Carbonell, M.B. Barbaro, C. Wilkin, Nucl. Phys. A **529**, 653 (1991).
14. D. Chiladze *et al.*, Phys. Lett. B **637**, 170 (2006).
15. D. Chiladze *et al.*, Phys. Rev. ST Accel. Beams **9**, 050101 (2006).
16. M.B. Barbaro, C. Wilkin, J. Phys. G **15**, L69 (1989).
17. S. Barsov *et al.*, Nucl. Instrum. Methods A **462**, 364 (2001).
18. R. Maier *et al.*, Nucl. Instrum. Methods A **390**, 1 (1997).
19. A. Khoukaz *et al.*, Eur. Phys. J. D **5**, 275 (1999).
20. A. Kacharava *et al.*, *Measurement of the* $\vec{d}\vec{p} \to \{pp\}n$ *charge-exchange reaction with polarised beam and target*, COSY proposal **172** (2007).
21. K. Grigoryev *et al.*, AIP Conf. Proc. **915**, 979 (2007).
22. K. Grigoryev *et al.*, Nucl. Instrum. Methods A **599**, 130 (2009).
23. M. Mikirtychyants *et al.*, Nucl. Instrum. Methods A (2013) doi: 10.1016/j.nima.2013.03.043.
24. D. Mchedlishvili *et al.*, J. Phys.: Conf. Ser. **295**, 012099 (2011).
25. R. Engels *et al.*, AIP Conf. Proc. **980**, 255 (2008).
26. F. Rathmann *et al.*, AIP Conf. Proc. **675**, 553 (2003).
27. M. Mikirtychyants *et al.*, J. Phys.: Conf. Ser. **295**, 012148 (2011).
28. H.J. Stein *et al.*, At. Energy **94**, 24 (2003) and H.J. Stein *et al.*, in *Proceedings of the 18th Conference on Charged Particle Accelerators (RUPAC 2002)*, edited by I.N. Meshkov Vol. **1** (NRCRF, Obninsk, 2004) p. 220, `arxiv.org/abs/1101.5963/`.
29. V. Kamerdzhiev *et al.*, Nucl. Instrum. Methods A **532**, 285 (2004).
30. S. Dymov *et al.*, Part. Nucl. Lett. **1**, 40 (2004).
31. I. Fröhlich *et al.*, PoS **ACAT2007**, 076 (2007).
32. M. Lacombe *et al.*, Phys. Lett. B **101**, 139 (1981).
33. R.A. Arndt, I.I. Strakovsky, R.L. Workman, D.V. Bugg, Phys. Rev. C **48**, 1926 (1993).
34. S. Agostinelli *et al.*, Nucl. Instrum. Methods A **506**, 250 (2003) `http://geant4.web.cern.ch/geant4/`.
35. D. Mchedlishvili, PoS **STORI'11**, 040 (2011) `http://pos.sissa.it/`.
36. G.G. Ohlsen, Rep. Prog. Phys. **35**, 717 (1972).
37. R. Schleichert *et al.*, IEEE Trans. Nucl. Sci. **50**, 301 (2003).
38. S. Barsov, D. Mchedlishvili, C. Wilkin, *Measurement of spin observables in* $\vec{p}\vec{d}$ *elastic and inelastic scattering with polarised beam and target at ANKE-COSY*, COSY proposal **218** (2013).